True Polar Wander as a Mechanism for Second-Order Sea-Level Variations

Jon E. Mound* and Jerry X. Mitrovica

Long-term wander of the rotation pole can be a significant contributor to second-order (time scales of ~100 million years) sea-level variations. Numerical predictions based on realistic viscoelastic Earth models and paleomagnetically constrained polar motion yield global-scale, differential sea-level trends that can be as large as ~200 meters. From the results presented here, it is argued that the well-documented, second-order, Cretaceous-Tertiary sea-level cycle should be reinterpreted as some combination of a eustatic and a regionally varying rotational signal.

Global-scale, second-order (*1*) sea-level variations are well documented (*2–4*); however, the geophysical mechanism for these variations remains uncertain. One clue is that the well-known Cretaceous sea-level transgression apparently occurred when the mean rate of spreading at midocean ridges increased (*5*). This correlation has led to the view (*6*) that a change in the rate of plate creation alters the net volume of ocean basins and leads to global (that is, eustatic) sea-level fluctuations. But changes in the spreading rates of midocean ridges are also linked to subduction-induced sea-level variations that can be both eustatic (*7*) and regional (*7, 8*). Thus, the extent to which variations in plate motions have influenced eustatic sea-level trends over geological history is unclear. In this report, we argue that a significant portion of long-term sea-level variations may be a consequence of the response of the solid earth and oceans to slow changes in the orientation of Earth's rotation vector.

As a case study, we focus on the last 130 million years (My) (that is, the Cretaceous onward). One estimate of global sea-level change during this period (Fig. 1) is based primarily on data from seismic stratigraphy (*2, 4*). Although interpreted as a measure of global sea-level change, the long-term trend shown by the curve and others of its kind (*9*) are generally based on data from few, and relatively localized, geographic regions. [Shorter term sea-level variations are inferred from a wider distribution of sites (*2, 4*).] The methodology used to construct the curve is also rather contentious (*10*); nevertheless, we use the curve as a workable estimate of the size and sense of the second-order sea-level cycle over the last 130 My. The inferred trend is characterized by a sea-level rise (transgression) of ~100 m during the Cretaceous followed by a gradual sea-level fall (regression) to the present.

Department of Physics, University of Toronto, 60 Saint George Street, Toronto, M5S 1A7, Canada.

*To whom correspondence should be addressed.

Eardley (*11*) argued that tidal deceleration of Earth's rotation rate was sufficient to produce a pole-to-equator sea-level change of ~400 m over the last 100 My and that this effect could account for an apparent latitudinal dependence in sea-level trends. A subsequent analysis (*12*) reduced this estimate to ~100 m. Mörner (*13*) argued (qualitatively) that the apparent latitudinal dependence in long-term sea-level trends may arise from the influence of "rotational tilt" [that is, true polar wander (TPW)]. Sabadini and colleagues (*14*) showed that relatively rapid episodes of TPW (of ~1° per million years) may influence or control third-order sea-level cycles (*1*).

In our study we incorporated geologically inferred TPW paths into the quantitative analysis. Through comparison of hot spot tracks, paleomagnetic measurements, and kinematic plate reconstructions, TPW paths can be reconstructed over geological time (*15, 16*) (Fig. 2). Because there can be significant disagreements in the inferred TPW path before 130 million years ago (Ma) (*15, 16*), we limited our calculations to the latter time span. From 120 to 50 Ma the rotation pole moved away from North America at ~0.4° per million years. From 30 to 0 Ma the pole reversed direction in the hot-spot reference frame. To specify completely the rotation vector of Earth over the last 130 My, we also required an estimate of the length of day over this time interval. We adopted a geologically inferred time series of tidal deceleration (*17*).

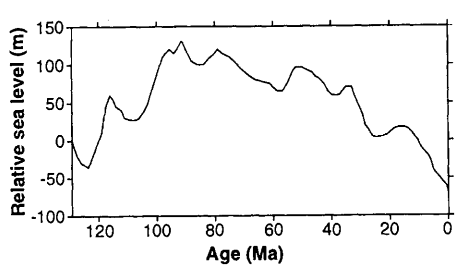

Fig. 1. A long-term sea-level curve inferred from seismic stratigraphy (*4*). We adopted the oldest datum on the plot as the zero for the relative sea-level fluctuation.

The spatial geometry of rotation-induced changes in sea level has been discussed by a number of investigators (*14, 18, 19*). Variations in the rotation rate (Fig. 3A) induce a latitudinal sea-level perturbation; tidal deceleration increases sea level at high latitudes and decreases it at low latitudes. TPW-induced sea-level changes are more complicated (Fig. 3B). In this case, the sea-level perturbation is zero on two great circles (dashed lines in Fig. 3B): the first at 90° from the instantaneous pole of rotation, and the second oriented perpendicular both to the first great circle and to the instantaneous great circle path of the pole. These two great circles define four quadrants (*20*). When the local rotation pole (that is, the north pole in the Northern Hemisphere and the south pole in the Southern Hemisphere) is moving toward a quadrant, sea level falls in that quadrant. Conversely, when the local rotation pole is moving away from a quadrant, sea level rises in that quadrant. The great circles of zero sea-level change associated with the mean motion of the rotation pole over the past 10 My lie roughly on the equator and the great circle defined by 51°E and 231°E (Fig. 3C).

A comparison of Figs. 1, 2, and 3 suggests that TPW may have influenced the second-order, sea-level cycle over the last 130 My. The change in the direction of TPW at ~50 Ma roughly coincides with the reversal in the long-term sea-level trend (*21*). Quadrants containing sites in North

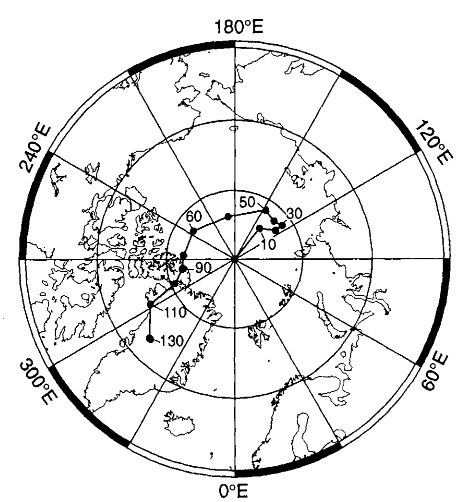

Fig. 2. Locations of the north rotation pole (solid circles) in the hot spot reference frame over the last 130 My [adapted from (*16*)] superimposed on the present-day coastline geometry. The axes of the 95% confidence ellipses associated with the individual pole positions are estimated in (*16*) to be ~5°. The pole position is relatively unchanged from 130 to 120 Ma.

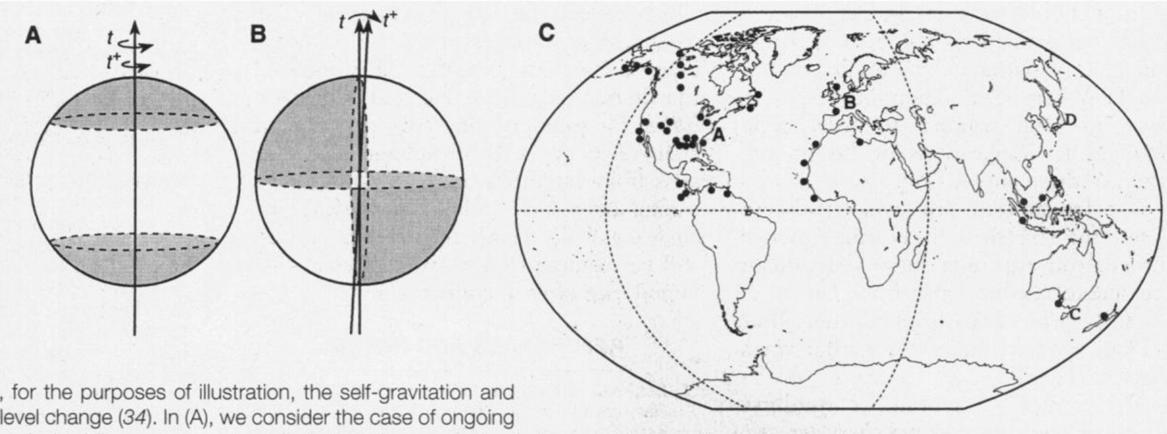

Fig. 3. Schematic illustration of the approximate spatial geometry of sea-level changes induced by perturbations in the magnitude (**A**) or orientation (**B**) of Earth's rotation vector from time t to t^+. The shaded regions represent areas of sea-level rise, and the unshaded regions represent areas that experience a sea-level fall. In constructing these simple figures, we neglected, for the purposes of illustration, the self-gravitation and loading effects of the sea-level change (*34*). In (A), we consider the case of ongoing tidal deceleration, and the dashed lines represent small circles of zero sea-level change. Mathematically, the spatial dependence may be expressed (approximately) as the surface spherical harmonic of degree two and order zero. The sea-level rise at the pole is roughly twice the magnitude of the equatorial sea-level fall. In (B), the dashed lines are great circles of zero sea-level change for the case of a small clockwise shift of the rotation vector. In this case the sea-level distribution is given (approximately) by the surface spherical harmonic of degree two and order one, and the maximum sea-level change is obtained at 45° from the poles (*20*). (**C**) The dotted lines represent great circles of zero TPW-induced sea-level variation associated with the mean TPW path over the last 10 My. The collection of continents within each quadrant is not significantly altered either by the reorientation of the quadrants over the last 130 My (as polar wander proceeded) or by plate motions. Sites used in the seismic stratigraphic analysis (*2*) of short-term (third-order and higher) sea-level trends are shown by solid circles and letters A through D. The letters are used to identify sites considered in Fig. 4.

America, Europe, North Africa, and Australia should have experienced some amount of TPW-induced sea-level rise from 130 to 50 Ma (as the local pole moved away from these quadrants) followed by a sea-level fall since 50 Ma (as the pole changed direction in the hot-spot frame), consistent with the geological record of sea-level change over the same period (Fig. 1). The trend would be reversed for sites in the remaining two quadrants.

To quantify the TPW effect, we computed gravitationally self-consistent sea-level change driven by long-term variations in the rotation vector (*16, 17*) of spherically symmetric, viscoelastic Earth models (*22*). These models have a realistic elastic structure (*23*), an elastic lithosphere, and isoviscous upper and lower mantle regions (*24*). The lithospheric thickness and the upper and lower mantle viscosities, which we denote by LT, ν_{UM}, and ν_{LM}, respectively, are free parameters. The time scale being considered (the last 130 My) requires that we incorporate plate motions to prescribe the evolution of both ocean distribution (*25*) and site locations (*26*).

In our initial calculation of second-order sea-level variations (Fig. 4), we adopted an Earth model previously used to consider shorter time scale effects of TPW (*14*). In all cases the contribution to the sea-level variation from changes in the rotation rate (compare the solid and dotted lines) was minor and significantly less than has been suggested (*11, 12*). We conclude that TPW-induced sea-level effects dominate the total sea-level prediction (*27*). The sense of the predicted sea-level perturbation was positive for the North American, European, and Australian sites and negative for the site in Japan. The sea-level fluctuation predicted for the North American site is ~50 m for this particular Earth model. The predicted sea-level changes for the European and Australian sites are smaller by about a factor of 2. This difference reflects the TPW path (Fig. 2), which produces a significantly larger change in the rotational colatitude (*28*) of the North American site than, for example, the site in Europe.

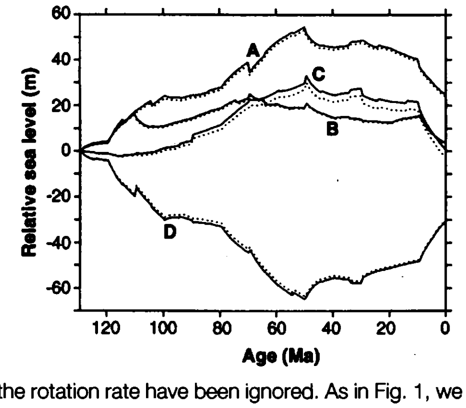

Fig. 4. Predicted rotation-induced sea-level change (solid lines) for four sites (A through D) in Fig. 3C. In the calculations we adopted the TPW path shown in Fig. 2 and the time series of rotation rate changes described in (*17*). The viscoelastic model is adopted from (*14*); it is characterized by a lithospheric thickness of 100 km, and upper and lower mantle viscosities of 10^{21} and 30×10^{21} Pa-s, respectively. The present-day geographic coordinates of the sites are as follows: curve A, 35°N, 76°W (North America); curve B, 50°N, 10°E (Europe); curve C, 40°S, 148°E (Australia); and curve D 36°N, 138°E (Japan). However, the predictions include the influence of continental drift on site locations. The dotted line for each curve is analogous to the solid line, except that changes in the rotation rate have been ignored. As in Fig. 1, we plot sea-level fluctuations relative to the value at 130 Ma.

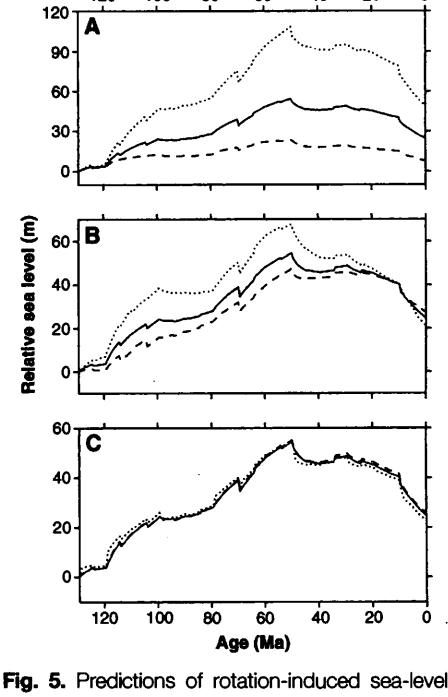

Fig. 5. Predictions of rotation-induced sea-level change for the North American site (as in Fig. 4, curve A). The calculations involve a suite of viscoelastic Earth models that systematically vary the free parameters of the model specified in Fig. 4 (LT = 100 km, $\nu_{UM} = 10^{21}$ Pa-s, $\nu_{LM} = 30 \times 10^{21}$ Pa-s). (**A**) Lithospheric thicknesses of either 50 km (dashed line), 100 km (solid line), or 200 km (dotted line). (**B**) Upper mantle viscosities of either 5×10^{20} Pa-s (dashed line), 10^{21} Pa-s (solid line), or 2×10^{21} Pa-s (dotted line). (**C**) Lower mantle viscosities of either 10×10^{21} Pa-s (dashed line), 30×10^{21} Pa-s (solid line), or 100×10^{21} Pa-s (dotted line).

In addition to second-order sea-level trends, our predictions also include shorter time-scale variations. This result confirms that TPW may be an important mechanism for third-order, regional sea-level cycles (*14*) and has implications for the interpretation of these curves (*29*).

The longer term sea-level trends predicted for the sites in North America, Europe, and Australia show a significant Cretaceous sea-level rise from 130 to 50 Ma, followed by a sea-level fall that offsets a dominant portion of the earlier transgression (Fig. 4).

The predicted amplitude of the differential second-order signal between the North American and Japanese sites exceeds 100 m (Fig. 4). This prediction will be dependent on the viscoelastic Earth model that is used. There is a growing consensus that mantle viscosity increases with depth by a factor close to the value we adopted in constructing Fig. 4 (*30*). Reasonable variations in either the upper or the lower mantle viscosity of the adopted model do not produce significant changes in the predicted TPW-induced, sea-level signal (Fig. 5, B and C). The predictions are, however, sensitive to variations in the adopted lithospheric thickness (Fig. 5A). Doubling this thickness increases the predicted sea-level fluctuation for the North American site by a factor of 2 to ~100 m, which is comparable with the estimated second-order signal (Fig. 1) (*31*). In the case of the thicker lithosphere, the differential sea-level signal between North America and Japan is also doubled to ~200 m.

Our modeling does not include lateral variations in Earth structure, and hence the appropriate choice for LT in our calculations is unclear. A value of $LT > 100$ km would not be unreasonable. For example, the North American craton is thought to have a thick continental root (*32*). Furthermore, many sites used in sea-level analyses are on stable continental margins in proximity to old oceanic lithosphere.

Our results suggest that TPW-induced sea-level changes can contribute significantly to second-order sea-level cycles. Furthermore, TPW effects cannot be ignored when one is comparing or combining sea-level data from different geographic regions. The often-cited correlation between spreading rates and sea-level fluctuations (*5*) is consistent with a sizeable TPW-induced sea-level signal. Recent modeling studies (*33*) have shown that the observed TPW path is consistent with predictions obtained by back-advecting seismically inferred density heterogeneities. Thus, TPW speeds (and the associated sea-level fluctuations) are likely linked to spreading rates, which reflect the rate of advection. The second-order sea-level cycle since 130 Ma is likely a combination of a TPW-induced (quadrant-localized) signal and a eustatic trend, for example, one that depends on changes in ocean basin volume that may arise from variations in spreading rates. A careful analysis of sea-level data, which include a globally distributed network of sites, will be required to distinguish the relative importance of each contributor.

REFERENCES AND NOTES

1. Sea-level variations, as reflected in stratigraphic cycles, are classified in terms of their duration. For example, following A. D. Miall [*Principles of Sedimentary Basin Analysis* (Springer-Verlag, New York, 1990)], we define second-order cycles as lasting 10 million to 100 million years and third-order cycles as lasting 1 million to 10 million years.
2. P. R. Vail, R. M. Mitchum, S. Thompson III, *Am. Assoc. Petrol. Geol. Mem.* **26**, 83 (1977).
3. A. Hallam, *Palaeogeogr. Palaeoclimatol. Palaeoecol.* **23**, 1 (1978).
4. B. U. Haq, J. Hardenbol, P. R. Vail, *Science* **235**, 1156 (1987).
5. J. D. Hays and W. C. Pitman, *Nature* **246**, 18 (1973).
6. D. L. Turcotte and G. Schubert, *Geodynamics* (Wiley, New York, 1982).
7. M. Gurnis, *Science* **250**, 970 (1990).
8. J. X. Mitrovica, C. Beaumont, G. T. Jarvis, *Tectonics* **8**, 1079 (1989); M. Gurnis, *Geology* **21**, 29 (1993); *Nature* **364**, 589 (1993); J. X. Mitrovica *et al.*, *Geodynamics* **22**, 79 (1996).
9. A. B. Watts and M. S. Steckler, in *Deep Drilling Results in the Atlantic Ocean: Continental Margins and Paleoenvironment*, M. Talwani *et al.*, Eds. (*AGU Maurice Ewing Series 3*, American Geophysical Union, Washington, DC, 1979), pp. 218–234.
10. A. D. Miall (*1*), for example, has criticized the seismic stratigraphic method of sea-level analysis. An alternate method of estimating long-term eustatic sea-level trends involves a correlation of continental flooding events [for example, C. G. A. Harrison, in *Sea Level Change*, R. Revelle, Ed. (National Academy Press, Washington, DC, 1990), pp. 141–158]. This approach is susceptible to contamination from regional, tectonically driven, sea-level signals (*8*).
11. A. J. Eardley, *Am. Sci.* **52** (no. 4), 488 (1964).
12. S. M. Flatté, *J. Geophys. Res.* **70**, 5189 (1965).
13. N.-A. Mörner, *Geology* **9**, 344 (1981); *Cretaceous Res.* **1**, 329 (1980).
14. R. Sabadini, C. Doglioni, and D. A. Yuen [*Nature* **345**, 708 (1990)] considered the sea-level response of a radially stratified viscoelastic Earth subject to a constant polar wander of 1° per million years. Their calculations suggest that this level of TPW can produce ~20 to 50 m of sea-level change over 1 My.
15. J. A. Andrews, *J. Geophys. Res.* **90**, 7737 (1985).
16. J. Besse and V. Courtillot, *ibid.* **96**, 4029 (1991).
17. G. E. Williams, *J. Phys. Earth* **38**, 475 (1990); *Geophys. Res. Lett.* **24**, 421 (1997). Williams in the 1997 paper analyzed variations in the thickness of tidal rythmites and inferred that there were 401 ± 7 sidereal days per year at 620 Ma compared with the present value of 366.24 sidereal days per year. We assume that the change in the angular momentum over this time interval is linear in order to derive a variation in rotation rate over the last 130 My.
18. G. A. Milne and J. X. Mitrovica, *Geophys. J. Int.* **126**, F13 (1996).
19. In the context of TPW induced by glacial isostatic adjustment, see D. Han and J. Wahr, in *Slow Deformations and Transmission of Stress in the Earth*, S. C. Cohen and P. Vanicek, Eds. (American Geophysical Union, Washington, DC, 1989), pp. 1–6; (*18*); B. G. Bills and T. S. James, *Geophys. Res. Lett.* **23**, 3023 (1996).
20. TPW acts to perturb the centrifugal potential associated with Earth rotation. The geographically varying component of this potential has an ellipsoidal (that is, degree two and order zero) form. The perturbing potential is thus the difference between two ellipsoidal forms whose axes are offset by a slight rotation. This difference, and the sea-level change that results, has a geometry (Fig. 3B) that may be described by the surface spherical harmonic of degree two and order one (*14, 18, 19*). As polar wander proceeds, the instantaneous orientation of the quadrants of this surface spherical harmonic (see Fig. 3B) changes.
21. We found no previous mention of the obvious correlation between the sea-level trend in Fig. 1 and the sense of the polar motion evident in Fig. 2.
22. The equation governing this calculation is derived by G. A. Milne and J. X. Mitrovica (*18*) (see their equations A7 through A10). The minor adjustments required to consider the case of internally forced TPW are discussed below their equation A10. The sea-level equation we solve incorporates not only the effect of TPW on both the geoid and solid surface but also the self-gravitation and loading effect of a time-dependent ocean distribution.
23. We adopt the preliminary reference Earth model specified in A. M. Dziewonski and D. L. Anderson, *Phys. Earth. Planet. Inter.* **25**, 297 (1981).
24. The boundary between the upper- and lower-mantle region is taken to be at a depth of 660 km.
25. M. F. Coffin *et al.*, *Univ. Texas Inst. Geophys. Tech. Rep.* **122** (1992), p. 49.
26. Past changes in site location were derived from E. Irving, *Geophys. Surv.* **5**, 299 (1983).
27. It is straightforward to show that TPW-induced sea-level trends on a purely inviscid planet will be close to zero. The sea-level response of Earth to a perturbation in the imposed centrifugal potential is governed by the so-called h and k viscoelastic tidal Love numbers [P. Wu and W. R. Peltier, *Geophys. J. R. Astron. Soc.* **76**, 753 (1984)] at spherical harmonic degree two (*18*). In the time domain these numbers (which govern the deformation of the solid surface and the perturbation to the gravitational equipotential at the undeformed surface) have the following form:

$$h(t) = h^E\delta(t) + \sum_{k=1}^{K} r_k \exp(-s_k t) \qquad (1)$$

and

$$k(t) = k^E\delta(t) + \sum_{k=1}^{K} r'_k \exp(-s_k t) \qquad (2)$$

where the superscript E represents the elastic response, δ is the Dirac-delta function, and t is the time. The second term on each right side is the nonelastic response, and it is composed of a set of K normal modes of pure exponential decay. These normal modes are defined by inverse decay times s_k and amplitudes of either r_k or r'_k. If we consider, for simplicity, a discrete jump in the pole position at $t = 0$, then the time-domain dependence of the sea-level response will be governed by the function

$$\beta(t) = 1 + k^E - h^E + \sum_{k=1}^{K} \frac{r'_k - r_k}{s_k}[1 - \exp(-s_k t)] \qquad (3)$$

For times much longer than the decay times ($1/s_k$), the response can be obtained by taking the limit $t \to \infty$ through Eq. 3. This gives

$$\beta_\infty = 1 + k^E - h^E + \sum_{k=1}^{K} \frac{r'_k - r_k}{s_k} \qquad (4)$$

In the case of no elastic lithosphere, it is easy to verify, by using numerical calculation, that $\beta_\infty \sim 0$. Hence, the TPW-induced sea-level response on an inviscid planet is negligible. Physically, this result indicates that the bounding sea-level surfaces (the geoid and the solid surface) move together on an inviscid planet to a perturbation in the imposed centrifugal potential. A departure from a purely inviscid response can occur for one of two reasons. First, the existence of an elastic lithosphere will ensure that $\beta_\infty \neq 0$. Second, there

may be normal modes that have decay times sufficiently long that the modes retain some level of disequilibrium even for the time scale of TPW considered here [hence, $\beta(t)$ would not have relaxed to β_∞]. We have found that the dominant, normal-mode contribution arises from the so-called M1 mode. The M1 mode arises from a deflection of the density discontinuity at a depth of 660 km between the upper and lower mantle. Thus, excitation of the mode requires that the discontinuity behaves nonadiabatically (that is, effectively as a chemical boundary) on the time scales we are considering. If this is not the case, then the mode would not be excited and the M1 contribution would vanish. As an example, the peak ~54 m signal in Fig. 4 (curve A) has a contribution of ~43 m from the elastic lithosphere and ~11 m from the M1 mode.
28. We define rotational colatitude as the angular distance of a site from the instantaneous north pole of rotation.
29. In the seismic stratigraphic analysis of short-term (third-order cycles and higher) sea-level change (*2*, *4*), North American and European sites dominate (Fig. 3C). The relative proximity of these sites suggests that they will experience similar TPW-induced sea-level trends. Thus, as has been suggested (*14*), it is unclear to what extent eustatic versus (TPW-induced) quadrant-localized signals contribute to the mean third-order sea-level trends.
30. See, for example, B. H. Hager, *J. Geophys. Res.* **89**, 6003 (1984); M. A. Richard and B. H. Hager, *ibid.*, p. 5987; M. Nakada and K. Lambeck, *Geophys. J. Int.* **96**, 497 (1989); Y. Ricard and B. Wuming, *ibid.* **105**, 561 (1991); J. X. Mitrovica, *J. Geophys. Res.* **101**, 555 (1996); A. M. Forte and J. X. Mitrovica, *Geophys. Res. Lett.* **23**, 1147 (1996).
31. The sensitivity to *LT* apparent in Fig. 5A follows from the arguments in (*27*). Furthermore, we have found that the contribution of the M1 mode to the sea-level signal (*27*) is sensitive to variations in upper mantle viscosity, and less sensitive to variations in lower mantle viscosity, for this range of Earth models; this explains the results in Fig. 5, B and C.
32. T. H. Jordan, *Rev. Geophys.* **13**, 1 (1975); S. P. Grand, *J. Geophys. Res.* **92**, 14065 (1987); A. M. Forte, A. M. Dziewonski, R. J. O'Connell, *Science* **268**, 386 (1995).
33. B. M. Steinberger and R. J. O'Connell, *Nature* **387**, 169 (1997).
34. Our sea-level predictions include the direct gravitational attraction and the loading effect of sea-level variations (*22*). The spatial geometry of these effects depends on the distribution of oceans, and therefore the sea-level trends we predict are more complicated than the simple illustrations in Fig. 3 imply.
35. We thank J. Wahr and two anonymous referees for their reviews of this report. We also thank D. Rowley for helpful comments. We are grateful for the ocean-continent geometry data provided by the PLATES Project of the Institute for Geophysics of the University of Texas at Austin. The work of J.X.M. was funded by Natural Sciences and Engineering Research Council of Canada and was supported by the Canadian Institute for Advanced Research (Earth Systems Evolution Program).

22 September 1997; accepted 2 December 1997

Catalytic Galactose Oxidase Models: Biomimetic Cu(II)–Phenoxyl-Radical Reactivity

Yadong Wang, Jennifer L. DuBois, Britt Hedman,* Keith O. Hodgson,* T. D. P. Stack*

Biomimetic functional models of the mononuclear copper enzyme galactose oxidase are presented that catalytically oxidize benzylic and allylic alcohols to aldehydes with O_2 under mild conditions. The mechanistic fidelity between the models and the natural system is pronounced. Modest structural mimicry proves sufficient to transfer an unusual ligand-based radical mechanism, previously unprecedented outside the protein matrix, to a simple chemical system.

An important goal of bioinorganic chemistry is the development of small inorganic complexes that not only reproduce structural and spectroscopic features, but also function in a manner similar to their natural counterparts. Despite much effort, faithful examples of catalytically functional models are rare, especially when O_2 is used as the oxidant (*1*). Presented here is a family of functional models of galactose oxidase (GOase) that catalytically oxidize benzylic and allylic alcohols to aldehydes with O_2 under mild conditions. The structural design of the models follows directly from the structure of the active site of the enzyme, and the ligand-based radical mechanism elucidated here parallels that proposed for the native system. Considering that a chemical precedent for this radical-based reaction outside a protein matrix has been lacking, the structural, spectroscopic, and mechanistic fidelity of these model complexes relative to the native system is striking.

GOase (*2*, *3*), a mononuclear copper enzyme, couples the oxidation of alcohols to aldehydes with the reduction of O_2 to H_2O_2 (Eq. 1) through an unusual Cu(II) phenoxyl-radical active species (*2*, *4*). Despite the importance of this organic transformation, there are few highly efficient, environmentally benign synthetic catalysts (*5*). The development of catalytically functional GOase models (*6*) allows this radical mechanism (*2*) to be probed more readily and also may lead to efficient catalysts.

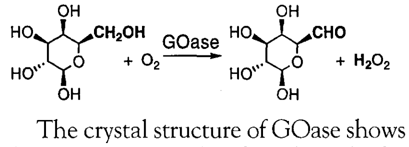

(1)

The crystal structure of GOase shows that the protein provides four ligands for the Cu(II) arranged in an unusual non-square–planar (nSP) coordination (Fig. 1A) (*7*): two tyrosine phenolates and two histidine imidazoles. A fifth exogenous H_2O ligand occupies an equatorial position in the Cu(II) square-pyramidal coordination. An interesting feature of this structure is a covalent thioether bond formed between a cysteine sulfur atom and an aromatic carbon of the equatorial phenolate ligand. It is this modified phenolate ligand that is thought to be oxidized to a radical, resulting in an electron paramagnetic resonance (EPR)–silent active form of the enzyme (*7*). The synthetic complexes reported here (Fig. 1B) possess a nSP Cu(II) N_2O_2 coordination geometry and appropriately positioned thioether substituents on the phenolate moieties (for BSI and BSP) (*8*). The x-ray crystal structure of one cupric complex, [Cu(II)BSI], confirms a nSP tetradentate ligation (Fig. 1C) (*9*), and EPR spectra of these Cu(II) complexes support a nSP geometry in solution as their $g_{||}$ values are significantly larger than those of the related square-planar Cu(II) complexes (*10*).

These complexes have spectroscopic characteristics similar to those of GOase. With respect to reactivity, the most important is the formation of a room-temperature (RT) stable, EPR-silent species upon one-electron (1 e^-) oxidation of each Cu(II) complex (*11*). We recently reported that *o,p*-substitution of the phenolate ring in these Cu complexes is critical to stabilizing their oxidized EPR-silent form (*8*). Oxidation of the Cu(II) complexes requires a strong oxidant, because their potentials range from +0.80 to +1.1 V (versus a standard calomel electrode) (*12*). In this process, the ligand **L**, not the metal, is oxidized (Eq. 2); the copper center remains Cu(II), as established by the similarity in energy of features in Cu K-edge x-ray absorption spectra (XAS) for [Cu(II)BDB] and its 1 e^- oxidized form—in particular, the $1s \rightarrow 3d$ pre-edge features at 8979 eV (Fig. 2) (*13*–*15*).

$$[Cu^{II}L] + NO^+(BF_4)^- \rightarrow [Cu^{II}L(BF_4)]^{\cdot} + NO\ (g) \qquad (2)$$

Y. Wang, J. L. DuBois, T. D. P. Stack, Department of Chemistry, Stanford University, Stanford, CA 94305–5080, USA.
B. Hedman, Stanford Synchrotron Radiation Laboratory, Stanford University, Stanford, CA 94309, USA.
K. O. Hodgson, Department of Chemistry, Stanford University, Stanford, CA 94305–5080, and Stanford Synchrotron Radiation Laboratory, Stanford University, Stanford, CA 94309, USA.

*To whom correspondence should be addressed. E-mail: hedman@ssrl.slac.stanford.edu; hodgson@ssrl.slac.stanford.edu; stack@leland.stanford.edu